Meteoritics & Planetary Science 38, Nr 2, 293–303 (2003)
Abstract available online at http://meteoritics.org

Numerical modeling of impact heating and cooling of the Vredefort impact structure

Elizabeth P. TURTLE,[1, 2*] Elisabetta PIERAZZO,[2] and David P. O'BRIEN[1]

[1]Lunar and Planetary Laboratory, University of Arizona, Tucson, Arizona 85721–0092, USA
[2] Planetary Science Institute, 620 North 6th Avenue, Tucson, Arizona 85705, USA
*Corresponding author. E-mail: turtle@lpl.arizona.edu

(Received 22 April 2002; revision accepted 25 March 2003)

Abstract–Large meteorite impacts, such as the one that created the Vredefort structure in South Africa ~2 Ga ago, result in significant heating of the target. The temperatures achieved in these events have important implications for post-impact metamorphism as well as for the development of hydrothermal systems. To investigate the post-impact thermal evolution and the size of the Vredefort structure, we have analyzed impact-induced shock heating in numerical simulations of terrestrial impacts by projectiles of a range of sizes thought to be appropriate for creating the Vredefort structure. When compared with the extent of estimated thermal shock metamorphism observed at different locations around Vredefort, our model results support our earlier estimates that the original crater was 120–160 km in diameter, based on comparison of predicted to observed locations of shock features. The simulations demonstrate that only limited shock heating of the target occurs outside the final crater and that the cooling time was at least 0.3 Myr but no more than 30 Myr.

INTRODUCTION

The Vredefort structure is the deeply eroded remnant of an ancient impact crater (e.g., Leroux, Reimold, and Doukhan 1994; Koeberl, Reimold, and Shirley 1996). It lies near the center of the Witwatersrand basin in South Africa and consists of a granite core 40–50 km in diameter surrounded by a 15–20 km wide ring of upturned, and in some places overturned, metasedimentary and metavolcanic strata. Estimates of the extent of vertical erosion that has occurred in the 2.023 ± 0.004 Gyr since the impact event (Kamo et al. 1996) range from 5 to 11 km (McCarthy, Stanistreet, and Robb 1990; Gibson and Wallmach 1995; Stevens, Gibson, and Droop 1997; Therriault, Grieve, and Reimold 1997; Gibson and Reimold 1999; Gibson 2002). Therefore, Vredefort provides us with an opportunity to observe the deeper structure of a very large impact crater.

Despite the extensive erosion that has occurred since the impact, it has been possible to infer the diameter of the original crater (see discussions in Turtle and Pierazzo 1998; Grieve and Therriault 2000). However, estimates range from 120–200 km, based on comparisons of observed and modeled locations of planar deformation features and shocked quartz (Turtle and Pierazzo 1998) and empirical relations between structural features at other terrestrial impact craters (Rondot 1994), to 250–350 km, based on scaling shock metamorphic and other features from observations at other terrestrial impact craters (Reimold and Wallmach 1991; Grieve and Masaitis 1994; Therriault, Grieve, and Reimold 1997), geophysical modeling (Henkel and Reimold 1998), and observations of thermal metamorphism (Gibson 2002). This wide range is due primarily to the extensive erosion that has occurred. Not only is the amount of erosion imprecisely known, but also, the deep structure of an impact crater this size is not well understood, making it difficult to scale from the present structure to the original crater diameter. Also, the degree to which the distribution of shocked quartz can be constrained is limited by the fact that not all of the lithologies near the Vredefort structure contain quartz crystals.

Such large impacts generate significant amounts of heat in the target which have important, long-term thermal implications. To investigate the degree and extent of the heating that occurs, we have analyzed the thermal results of numerical modeling performed previously to simulate the shock effects associated with large meteorite impacts (Turtle and Pierazzo 1998). Based on our earlier hydrocode models, we predicted temperatures during and after the passage of the impact-generated shock wave for a suite of projectile sizes spanning the range of diameter estimates for the Vredefort crater. Then, by combining the hydrocode results with Maxwell's Z-model for transient crater excavation (Maxwell and Seifert 1975) and our earlier finite-element models of crater collapse, we followed the displacement of shock isotherms through the formation of the final crater. Finally, we

performed thermal modeling to simulate the long-term cooling of the crater.

Based on the metamorphism observed in the rocks around Vredefort, Gibson, Reimold, and Stevens (1998) documented temperatures of ~673 K in samples from the mid-collar (at a distance of ~28 km from the structure's center), ~773 K in the inner-collar (~20 km from the center), and higher than 973 K but lower than 1173 K in the core (~8 km from the center). There are two factors that contribute to these temperatures. The first is heating by the shock wave that the impact generates. The second is that rock at the present surface was uplifted from greater depths later in the cratering process, so it was initially warmer than the surrounding rock. By comparing these observations with the temperatures in our simulations for different projectile sizes (and, therefore, different crater sizes), we have derived an independent estimate for the size of the crater.

NUMERICAL MODELING

The impact cratering process is usually divided into three stages (which, in reality, overlap to some degree): contact and compression (shock wave initiation and propagation), crater excavation, and crater collapse. Different physical processes dominate each of these stages, so we simulated each stage separately using techniques appropriate to their specific conditions. This procedure allowed us to follow the thermal evolution of the crater despite the disparate processes at work and the enormous variation in the timescales over which they operate. In our earlier work (Turtle and Pierazzo 1998), we used hydrocode modeling to simulate shock wave propagation during the contact and compression stage and into the excavation stage, the Z-model (Maxwell and Seifert 1975) to simulate the displacement of target material during the excavation stage, and finite-element modeling to simulate the distortion of the target material during the collapse of the transient crater. However, we only analyzed the shock pressures achieved in these simulations and their distribution for comparison to the observed locations of shock features around Vredefort. Here, we have analyzed the thermal aspects of the impact for comparison to more recent observations of thermal metamorphism (Gibson, Reimold, and Stevens 1998; Gibson and Reimold 1999; Gibson 2002). Furthermore, we have incorporated thermal modeling to extend our simulations and investigate the post-impact cooling of the final crater. We carried out our modeling procedure for a range of projectile diameters D_p = 10, 14, and 17 km, with impact velocities of 20 km/s. According to the scaling relation developed by Schmidt and Housen (1987), these simulations correspond to the formation of transient craters with diameters of D_{tc} ~80, 100, and 120 km, respectively. Transient craters of these sizes will collapse to final craters with diameter ranges of D_{fc} ~120–160, 150–200, and 185–240 km, respectively (e.g., Grieve, Robertson, and Dence 1981). For the purpose of illustrating our modeling sequence here, we show figures from the simulation with a 10 km diameter projectile.

Contact and Compression

We used the two-dimensional hydrocode CSQ (Thompson 1979) coupled with the semianalytical equation of state, ANEOS (Thompson and Lauson 1972), to model the contact and compression stage of the impact and the beginning of excavation (see detailed description of modeling procedure in Turtle and Pierazzo 1998). Axisymmetric simulations are sufficient for this work because, even during oblique impacts, symmetry is maintained at the depths (i.e., 5–11 km) that have been exposed by erosion since the impact at Vredefort (Pierazzo and Melosh 2000). Each simulation was run long enough to allow the shock to propagate in the target and degrade into a plastic stress wave (i.e., >10 s).

In hydrocode simulations, the actual target stratigraphy (Table 1) generally needs to be simplified to use materials for which equations of state have been developed. We modeled the target as a 14 km layer of quartzite (equation of state from Melosh, personal communication, 1996) to represent the quartzite-rich sedimentary layers (i.e., the Transvaal, Ventersdorp, and Witwatersrand supergroups) overlying a 31.5 km layer of granite (equation of state from Pierazzo, Vickery, and Melosh 1997), representing the granitic basement. Dunite (equation of state from Benz, Cameron, and Melosh 1989) was used to represent the mantle material beneath the continental crust. In addition, we used dunite for the projectile. Finally, we assumed a projectile velocity of 20 km/sec (typical of asteroid collisions with Earth [e.g., Bottke et al. 1994]). Spatial resolution was always kept at 20 cells per projectile radius (e.g., see Pierazzo, Vickery, and Melosh 1997 for a discussion on resolution). CSQ assumes axial symmetry, so the incidence angle was necessarily 90°, i.e., perpendicular to the target's surface. One hundred massless, Lagrangian tracer particles were distributed throughout the target to record the conditions of the material for the first ~15 seconds after impact. We interpolated between the tracer particles to determine the locations of contours of temperature change due to the impact-generated shock wave. Fig. 1 shows contours of temperature change, ΔT, due to the passage of the shock wave.

Excavation

The Z-model is an empirical relationship that predicts what material will be ejected during crater excavation as well as the displacement of the unejected material (Maxwell and Seifert 1975). This model assumes that the target material undergoes incompressible flow along stationary streamlines characterized by the parameter R_o, the radial distance at

Table 1. Target stratigraphy (somewhat simplified for modeling) and thermal parameters.

Unit (dominant lithology)	Approx. depth[a] (km)	Thermal conductivity[b] (W m^{-2} K^{-1})	Density[a] (kg m^{-3})	Heat production[b] (mW m^{-3})	Temperature[c] (at top of layer) (K)
Transvaal supergroup (Dolomite)	0–3.5	4.0	2800	1.92	273
Ventersdrop supergroup (Andesitic-Basaltic Lavas)	3.5–7.0	4.0	2900	1.92	347.5
Witwatersrand supergroup (Quartzite, Shale)	7.0–14	4.0	2650	1.92	416.1
Upper crust (Outer Granite Gneiss)	14–21	2.5	2650	3.0	535.6
Upper crust (Inlandsee Leucogranofels)	21–28	2.5	2650	1.82	678.6
Lower crust (Mafic Granulite)	28–38	2.5	2650	0.92	774.5
	38–44			0.17	871.2
Mantle (olivine)	>44	4.0	3300	0.0	920.4

[a]Reimold, personal communication (1990); Fletcher and Reimold (1989).
[b]Reimold, personal communication (1990); Jones, (1988); Nicolaysen, Hart, and Gale (1981); Values are consistent with those from Gibson and Jones (2002) which were not available at the time of modeling.
[c]Calculated.

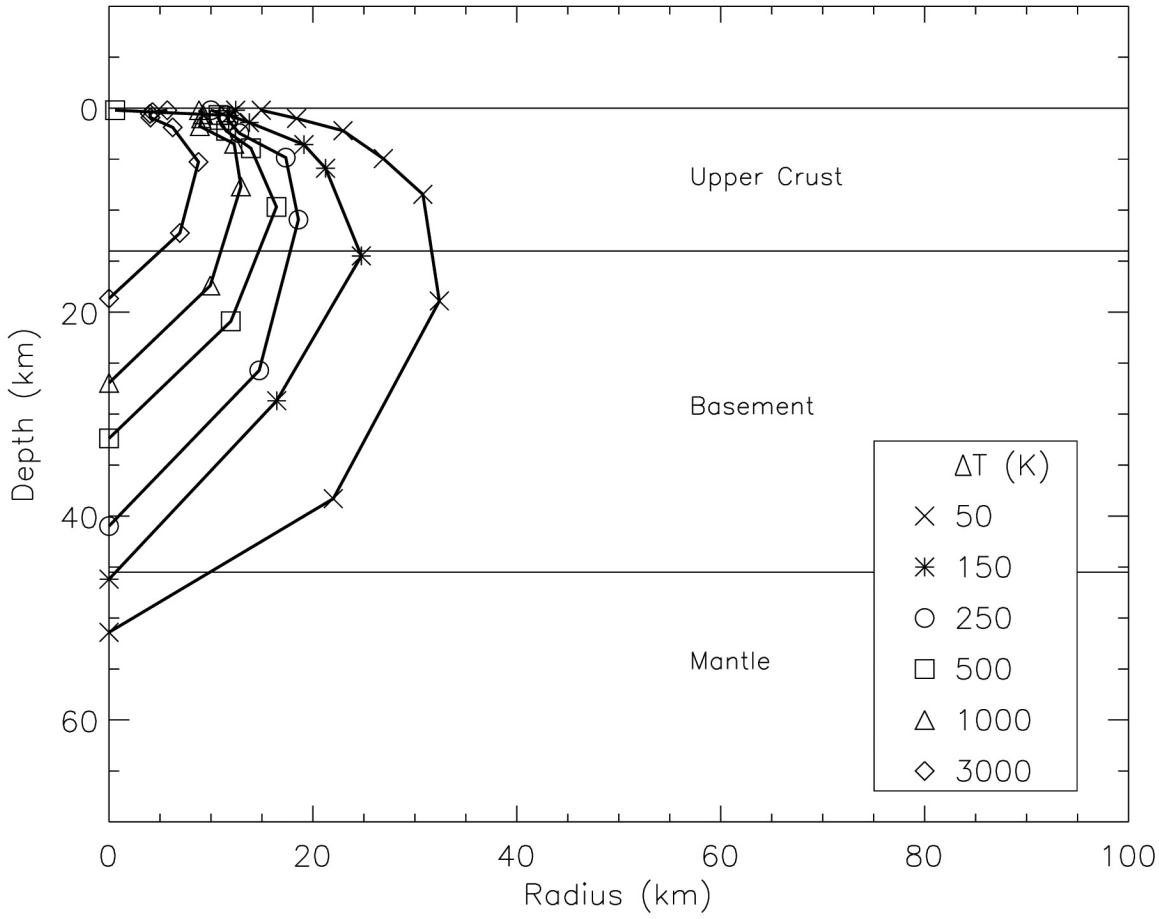

Fig. 1. Contours of shock-induced ΔT after the passage of the shock wave but prior to crater excavation (our hydrocode simulations cover the first 14.6 s of the impact) for our simulation of an impact by a 10 km diameter projectile. Thin, solid, horizontal lines illustrate the initial (simplified) stratigraphy.

which a streamline intersects the original surface. In polar coordinates the streamline equation is:

$$R = R_o (1 - \cos\theta)^{1/(Z-2)}$$

where R is radial distance, θ is the angle measured from the vertical axis, and Z ~3 (Maxwell and Seifert 1975). We used this relationship to determine the deformation of the target through the excavation stage. Fig. 2 shows the contours of temperature change from Fig. 1 after they have been distorted by the excavation flow that produced a transient crater 80 km in diameter and 24 km deep (corresponding to our simulation of an impact by a 10 km diameter projectile). For reference, Fig. 2 also illustrates the post-excavation positions of the Moho and other prominent stratigraphic boundaries (Table 1). It should be noted that for terrestrial craters of this size, the transient crater is a theoretical concept that represents the maximum extent of excavation. In reality, a transient crater this size would not have this shape at any single instant in time; the transient crater achieves its maximum depth, and rebound (i.e., crater collapse) begins before its horizontal excavation is complete.

Collapse

To model the collapse of the transient crater, we used the axially symmetric, visco-elastic version of Tekton, a finite-element code specifically designed for use in geophysical problems (Melosh and Raefsky 1980). We designed a mesh using material properties and rheologic parameters appropriate to the major stratigraphic units at Vredefort (Table 1). As for the hydrocode modeling, it was necessary to simplify the stratigraphy to lithologies for which the required rheologic parameters have been measured: limestone (Schmid, Boland, and Paterson 1977) for the Transvaal supergroup; diabase, quartzite, and granite (Kirby and Kronenberg 1987) for the Ventersdorp and Witwatersrand supergroups and the crystalline basement, respectively; and olivine (Goetze 1978) for the mantle. We also incorporated a hemispherical zone with a diameter twice that of the transient crater (i.e., roughly the size of the final crater) in which a low-viscosity, Newtonian rheology simulates material that is acoustically fluidized by the impact (Melosh 1977, 1982). Fig. 3a shows the locations of the

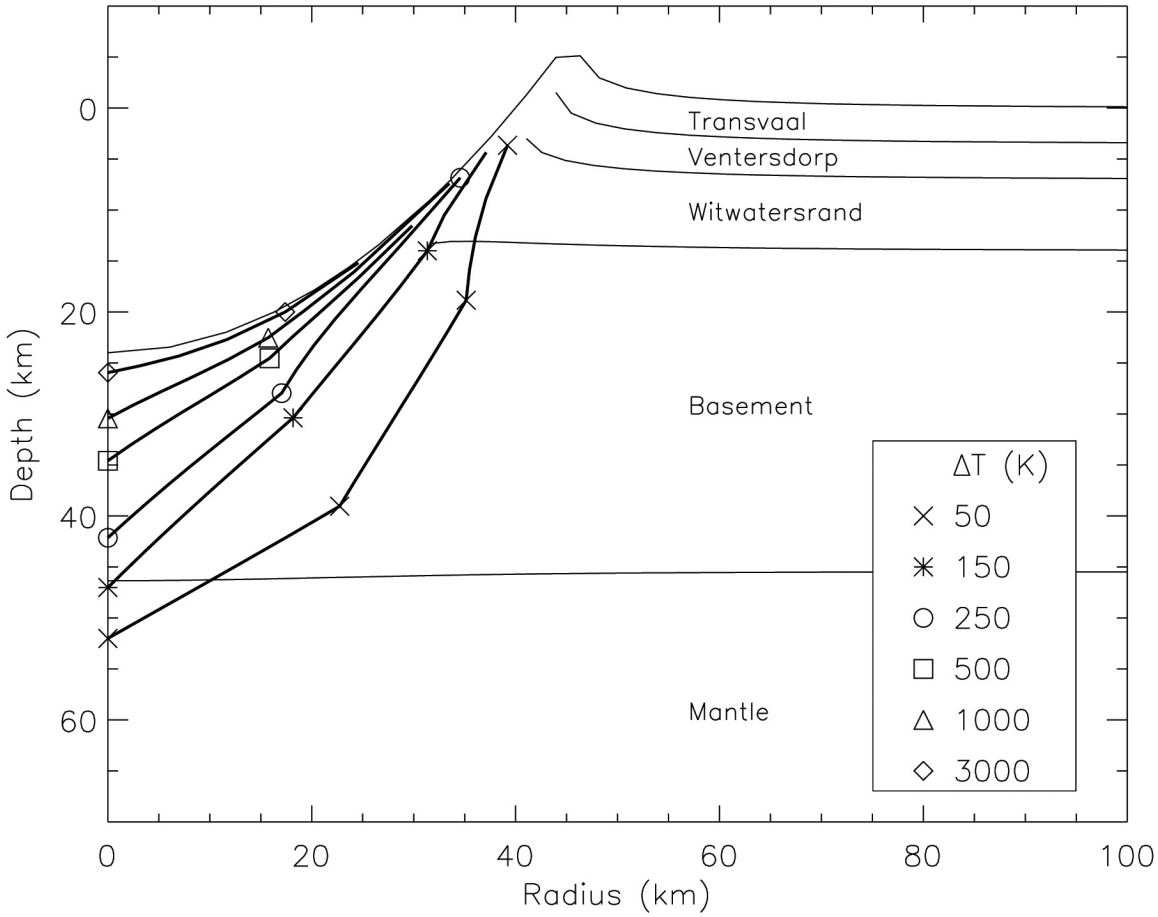

Fig. 2. Contours of post-shock ΔT after crater excavation. The thin lines show the surface of a transient crater 80 km in diameter and 24 km deep, which is predicted by Schmidt and Housen's (1987) scaling relation for a 10 km diameter projectile with an impact velocity of 20 km/s, and the post-excavation positions of prominent stratigraphic boundaries.

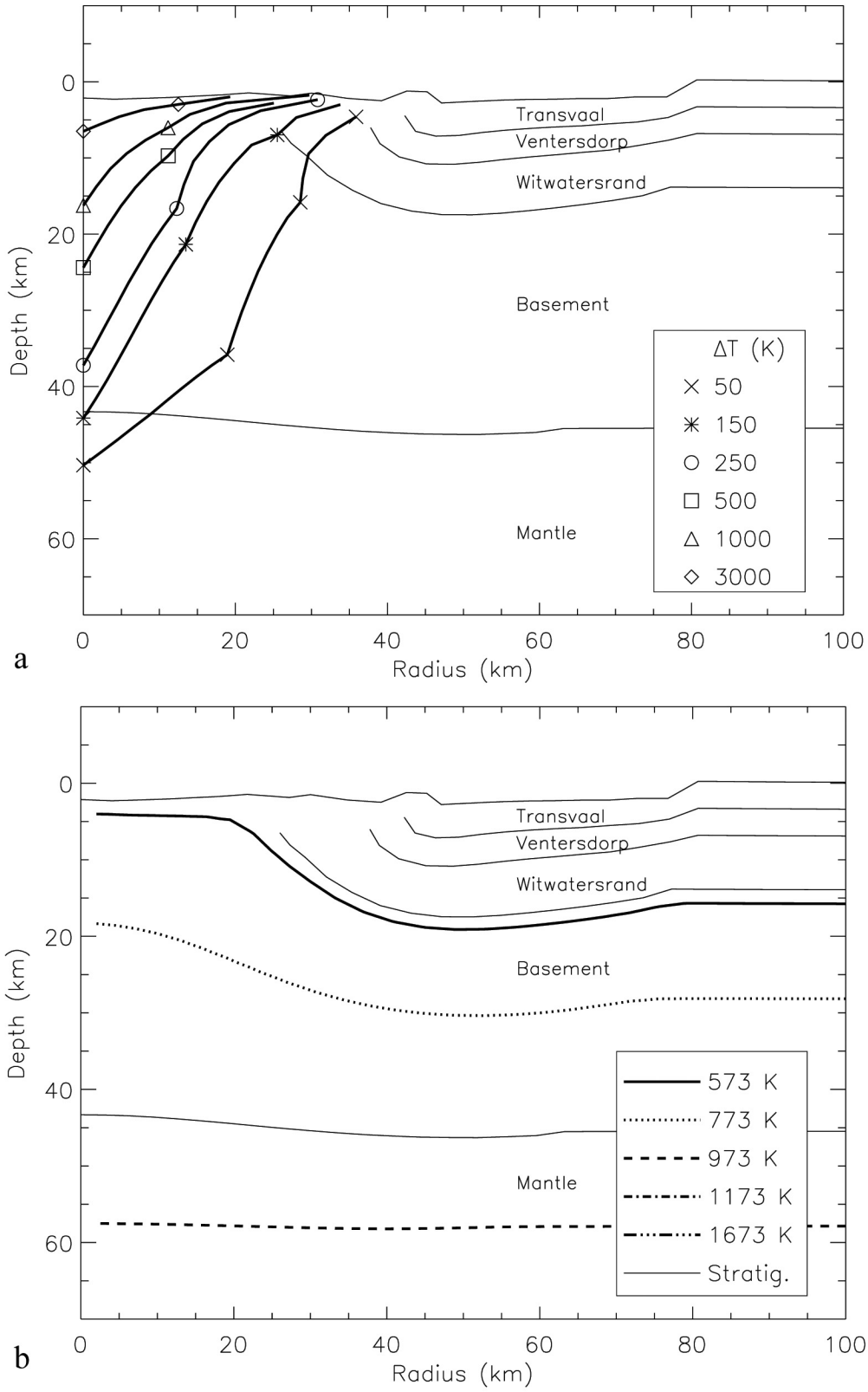

Fig. 3. Contours of: a) post-shock ΔT; and b) uplifted geothermal temperatures after crater collapse for the impact simulation with D_p = 10 km. The thin, solid lines show the surface of the final crater and the post-collapse positions of prominent stratigraphic boundaries. The small topographic high between 40 and 45 km radius is the unrelaxed remnant of the transient crater rim. It is not a peak ring (see text).

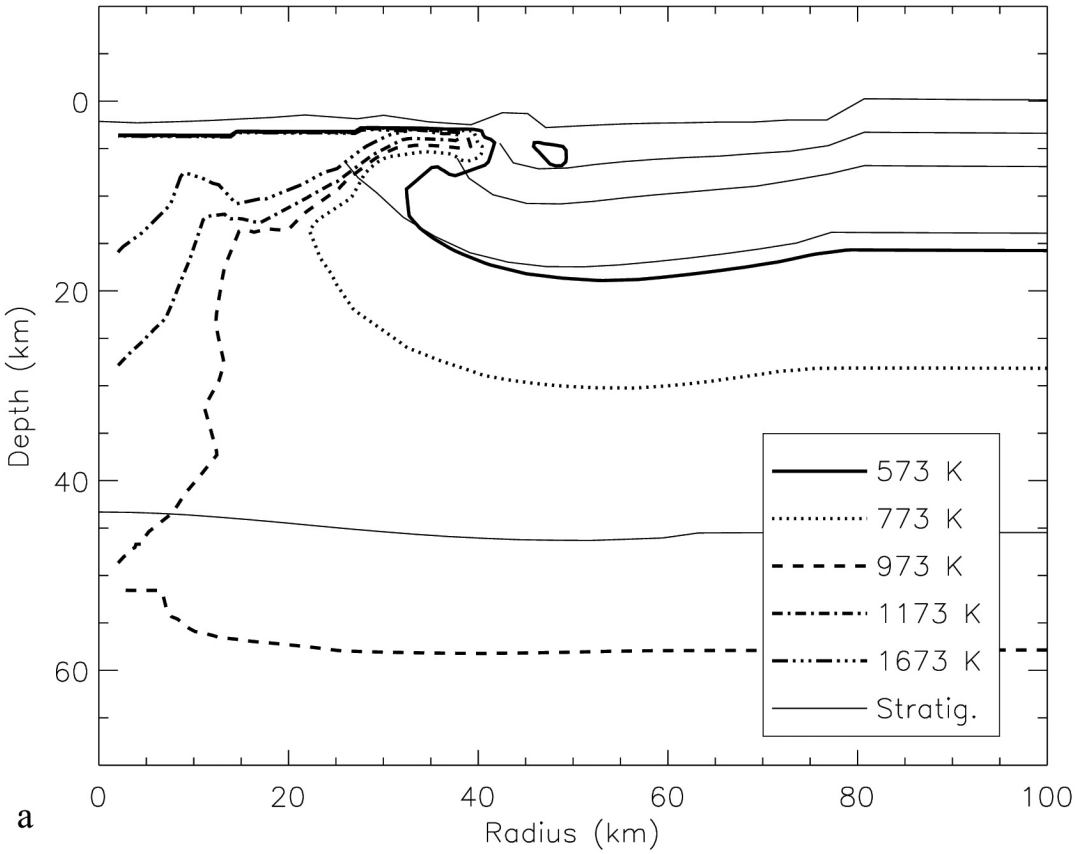
0
20
40
60
Depth (km)
0
20
40
60
80
100
Radius (km)
573 K
773 K
973 K
1173 K
1673 K
Stratig.

a

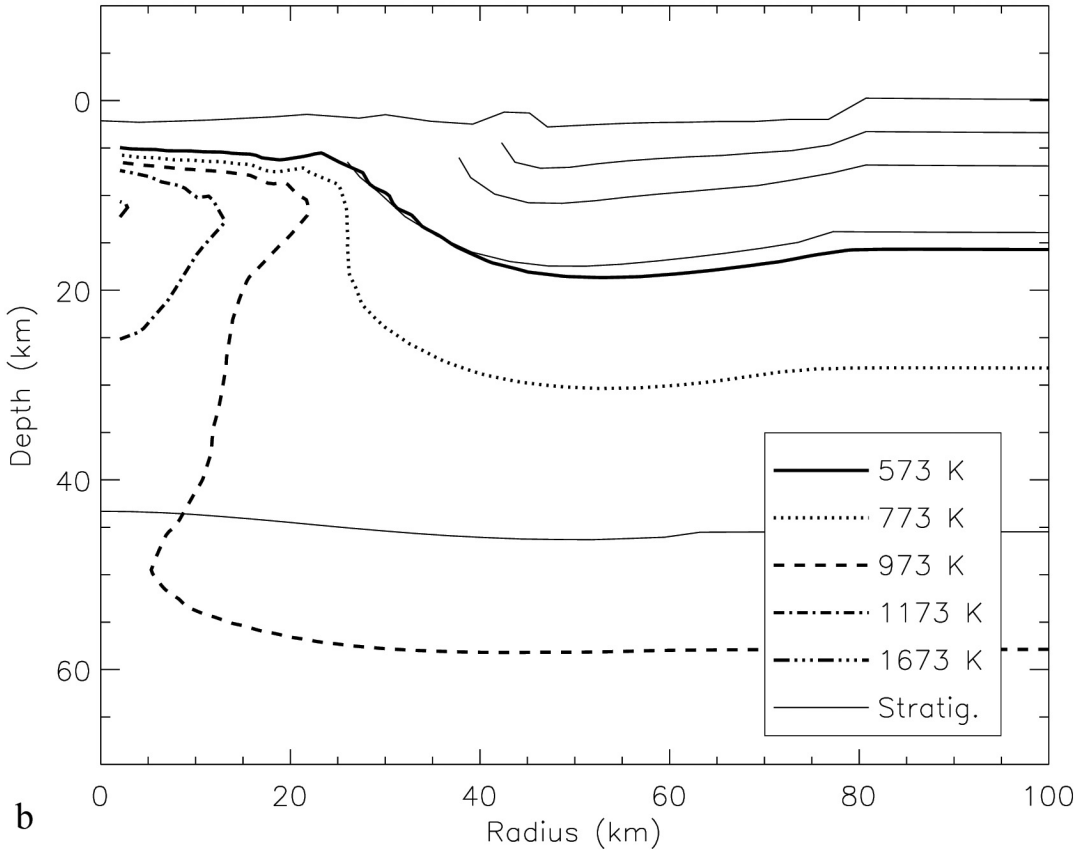
0
20
40
60
Depth (km)
0
20
40
60
80
100
Radius (km)
573 K
773 K
973 K
1173 K
1673 K
Stratig.

b

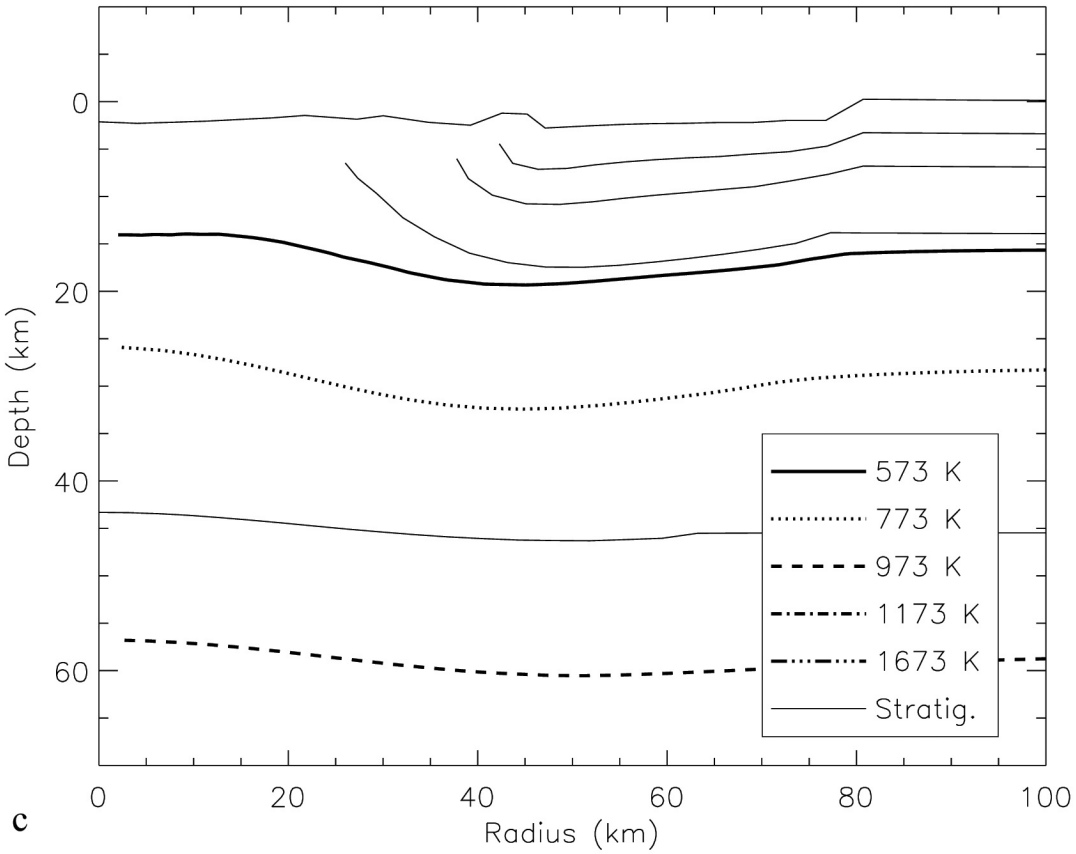

Fig. 4. Contours of total temperature due to both shock heating and uplift: a) immediately after collapse; b) 0.3 Myr after collapse; and c) 30 Myr after collapse. Cooling is by radiation and forced convection at the surface, and heat transport within the rock is by conduction. By 0.3 Myr, the surface has cooled to equilibrium with the atmosphere, but a steep temperature gradient remains below the surface. By 30 Myr, the crater has cooled completely to its equilibrium temperature profile. Thin, solid lines show the surface of the final crater and the post-collapse positions of prominent stratigraphic boundaries. The isotherms are somewhat curved due to the deformation of the different stratigraphic layers (which have different thermal properties) during the impact and collapse.

contours of temperature change due to the shock wave immediately after the transient crater for the 10 km diameter projectile has collapsed to the final crater. Comparison to Fig. 2 illustrates how the material has moved upward and somewhat inward. Fig. 3b demonstrates the amount of central uplift beneath the crater floor by illustrating the post-collapse locations of initially flat-lying absolute temperature contours due to the local geothermal gradient (calculated based upon thermal properties of the Vredefort lithologies from Reimold, personal communication 1990; Jones 1988; Nicolaysen, Hart, and Gale 1981). Fig. 4a shows the total post-impact temperatures due to the combined contributions of shock heating and uplift. One limitation of our finite element model is that it does not include inertia. Therefore, motion ceases when the material reaches isostatic equilibrium, precluding formation of features such as central peaks and peak rings. This reduces the accuracy of the locations of temperature contours at the surface near the crater floor, but is not expected to introduce significant uncertainty at the depths of interest here (cf., Collins et al. 2002).

Post-Impact Cooling

We have adapted a thermal model developed by O'Brien, Geissler, and Greenberg (2001) to terrestrial conditions in order to follow the long-term thermal evolution of the crater. The initial conditions for the model are the temperatures of the different stratigraphic units (consistent with the relevant material properties: thermal conductivity, radiogenic heat production, and density [Table 1]) and the post-collapse temperature profile of the crater. (A few unejected tracer particles had temperatures in excess of 3600 K, the temperature of incipient vaporization for silicates [Pierazzo, Vickery, and Melosh 1997]. However, imposing a maximum temperature of 3600 K did not change the results.) The model is axially symmetric, with the lower and radial boundary temperatures fixed (the boundaries are placed far away from the crater where the temperature is unchanged after the impact and collapse, such that they do not influence the thermal evolution of the crater). In the model, a specific heat of 1 kJ/kg K (typical for rocks and rock-forming minerals, e.g., Tables 21, 23, and 24 in Dimitriyev et al. 1972) is used for all

of the materials. We performed simulations using specific heats of 0.5 and 2.0 kJ/kg K to confirm that varying these values over a realistic range did not have a strong effect on the long-term cooling times. Heat transport within the rock is purely conductive, and phase changes are not treated here (i.e., no latent heat of fusion). The cooling at the surface boundary is dominated by blackbody radiation to the atmosphere for temperatures over 973 K and by forced convection in the atmosphere for temperatures below this, following Keszthelyi and Denlinger (1996).

Fig. 4 shows the temperature distribution around the crater immediately after collapse (a), after 0.3 Myr (b), and after 30 Myr (c). Immediately after crater collapse (Fig. 4a), the hot surface begins to cool by radiation to the atmosphere. Heating is confined mainly to a region 50 km in radius around the impact point. At 0.3 Myr after collapse (Fig. 4b), the surface has cooled to essentially equilibrium with the atmosphere, but there is still a very steep thermal gradient beneath the surface (about 100 K/km) leading to a peak temperature of around 1400 K at a depth of 10–15 km below the center of the crater. There is very little conductive heating of the cooler rocks surrounding the crater—the vast majority of heat is conducted upwards and radiated or convected away to the atmosphere. By 30 Myr (Fig. 4c), the crater has cooled to its equilibrium temperature profile. Note that the isotherms are not perfectly straight, due to the fact that the different stratigraphic layers (with different thermal conductivities and radiogenic heat production) have been warped during the impact and collapse.

Including latent heat of fusion in the model would increase the cooling times in our simulations. The latent heat of fusion for rocks is ~400 kJ/kg and the specific heat is ~1 kJ/kg K (Turcotte and Schubert 1982), implying that melt solidification can release enough heat to offset a temperature decrease of ~400 K, therefore increasing the overall cooling time. As the rock that would be initially melted in our model (the surface melt sheet) cools by significantly more than 400 K, the inclusion of latent heat of fusion should increase our estimated cooling times by no more than a factor of two. On the other hand, water has a high latent heat of vaporization, ~2500 kJ/kg, and specific heat, ~4 kJ/kg K (Turcotte and Schubert 1982), making it a very effective cooling agent. Water can be vaporized as it circulates through the hot rock, thus absorbing (and transporting away) a large amount of heat. This effect is directly connected to convection as a mechanism of heat loss.

Convective heat loss could be introduced by hydrothermal circulation generated within the crater following the impact (Newsom 1980). Newsom et al. (1996) hypothesize an increase in cooling rates by a factor of up to 100 over a purely conductive scenario due to hydrothermal convection. This would lower the total cooling time for Vredefort in our model to 0.3 Myr. On the other hand, geologic evidence suggests that many terrestrial hydrothermal systems cool at a rate not much faster than the conductive rate because of low permeability (Cathles, Erendi, and Barrie 1997). This is attributed to a "self-sealing" effect due to minerals deposited by the hydrothermal system that decreases the permeability of the reservoir (as seen in drill holes in Yellowstone National Park, USA, Keith, White, and Beeson 1978; and at the Haughton impact structure, Canada, Osinski, Spray, and Lee 2001). Detailed modeling of impact-generated hydrothermal systems is clearly needed to constrain their effect on cooling rates. For now, we consider 0.3 Myr to be a reasonable lower limit, and our conductive cooling time of 30 Myr to be an upper limit for the cooling timescale of the Vredefort impact structure.

RESULTS AND CONCLUSIONS

Fig. 5 compares the results for our simulations with 10 km and 14 km diameter projectiles to the post-impact temperatures derived by Gibson, Reimold, and Stevens (1998). Estimates for the amount of erosion that has occurred in the Witwatersrand Basin over the past 2 Ga range from ~5 to 11 km (McCarthy, Stanistreet, and Robb 1990; Gibson and Wallmach 1995; Therriault, Grieve, and Reimold 1997; Gibson and Reimold 1999; Gibson 2002). So, the present surface should lie between the two horizontal solid lines in each plot.

The results of the simulation with the 10 km diameter projectile are roughly consistent with the observations at depths believed to be exposed at the surface today (Fig. 5a). In this case, the modeled 673 K contour is within 2 km of the radius at which a comparable metamorphic temperature has been documented at Vredefort ($r_{T = 673\ K}$ = 27.9 km [site 1 in Gibson, Reimold, and Stevens 1998]) within the expected range of the depth to today's surface. The 773 K and 1173 K contours come within 3 km of the radii at which these temperatures have been documented ($r_{T = 773\ K}$ = 20.0 km and $r_{973\ K \le T \le 1173\ K}$ = 8.1 km [sites 2 and 3 in Gibson, Reimold, and Stevens 1998]) at a depth of ~11 km.

For the simulation with the 14 km diameter projectile, the modeled temperature contours are far outside the radii at which the same temperatures are documented (Fig. 5b). Within the appropriate range of depths, the 673 K, 773 K, and 1173 K contours are ≥9 km, ≥11 km and ≥13 km, respectively, from the documented locations. Therefore, this simulation demonstrates that impacts which generate transient crater cavities larger than ~100 km in diameter cannot match the observed metamorphism regardless of the level of erosion unless there is substantial uncertainty in the documented temperatures (on the order of a few hundred K) or their locations (on the order of 10 km).

When compared to the documented post-impact temperatures around Vredefort, these model results indicate that an impact which would produce a transient crater ~80 km in diameter (e.g., D_p = 10 km, v_{impact} = 20 km/s; Schmidt

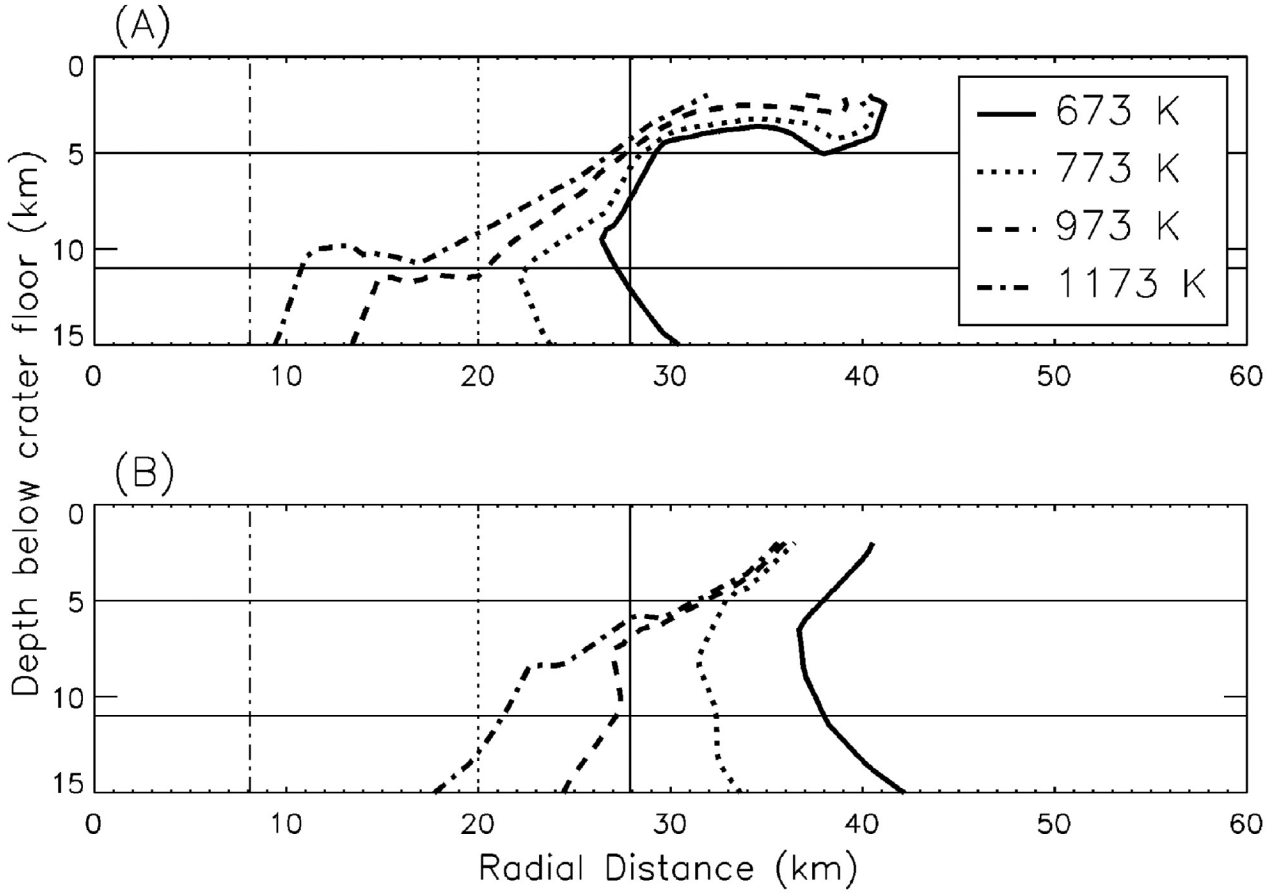

Fig. 5. Near-surface positions of the 673 K, 773 K, 973 K, and 1173 K contours for two impact simulations: a) D_{tc} ~80 km, D_{fc} ~120–160 km (D_p = 10 km, v_{impact} = 20 km/s); and b) D_{tc} ~100 km, D_{fc} ~150–200 km (D_p = 14 km, v_{impact} = 20 km/s). The vertical axis is the depth below the final crater floor, and the present surface is expected to lie between approximately 5 and 11 km (the region bounded by the thin, solid, horizontal lines). The vertical lines indicate the radii of sites where post-impact temperatures were determined by Gibson, Reimold, and Stevens (1998) to be ~673 K (solid vertical line), ~773 K (dotted vertical line), and between 973 and 1173 K (dot-dashed vertical line).

and Housen 1987) and a final crater ~120–160 km in diameter (Grieve, Robertson, and Dence 1981) is reasonably consistent with the observations. However, a transient crater ~100 km in diameter (e.g., D_p = 14 km, v_{impact} = 20 km/s; Schmidt and Housen 1987), which would produce a final crater ~150–200 km in diameter (Grieve, Robertson, and Dence 1981), is too large to be consistent with the observations. This conclusion is consistent with the estimate made by Turtle and Pierazzo (1998) for the size of the Vredefort crater, D_{fc} = 120–200 km, based on comparisons of the observed locations of shock features with simulation results. Despite the good agreement between our crater size estimates from comparisons to both shock pressures and post-impact temperatures, they are somewhat smaller than other diameter estimates which range from 200 km to as much as 300 km (e.g., Therriault, Grieve, and Reimold 1997; Henkel and Reimold 1996; Gibson 2002). These discrepancies may be due, at least in part, to assumptions about the shapes of the shock pressure contours (which, in this study, are a direct product of our simulations) or uncertainties in the amount of erosion that has occurred, as well as uncertainties inherent in scaling from other, generally smaller, impact craters (see discussion in Turtle and Pierazzo 1998). Our simulations are somewhat limited by the lack of inertia in Tekton, which precludes the formation of a central peak or peak ring. However, the formation of a peak ring, which would be expected for a crater of this size, would serve to push high-temperature contours even further outward (cf., Collins et al. 2002), making it unlikely that our results underestimate the size of the crater.

Our simulations indicate that the timescale for conductive cooling of the crater was on the order of 30 Myr. Depending on the efficiency of hydrothermal circulation, the cooling time could have been shorter by two orders of magnitude. In addition, when compared to the final crater size (120–160 km), the temperature contours in Fig. 5 indicate that little heating occurs outside the final crater itself; the significant heating is confined to well within the final crater. Possible heating due to ejecta deposited outside the crater rim would have only affected surface rocks, which have long

since been removed by erosion. Therefore, any apparent impact-related metamorphism and the development of hydrothermal circulation would have been limited to within the final crater itself, making it doubtful that the 2.02 Ga impact event could have caused Witwatersrand-basin-wide metamorphism. This result is consistent with Gibson and Jones' (2002) conclusion that the 2.06 Ga Bushveld magmatic event is likely to have been responsible for the regional metamorphism that occurred within the Witwatersrand basin.

Acknowledgments–We thank Roger Gibson and Uwe Reimold for numerous useful discussions about Vredefort and Paul Buchanan and an anonymous reviewer for their helpful comments. This research was supported by NASA grant NAGW-9112. This manuscript is PSI contribution #362.

REFERENCES

Benz W., Cameron A. G. W., and Melosh H. J. 1989. The origin of the moon and the single impact hypothesis III. *Icarus* 81:113–131.

Bottke W. F. Jr., Nolan M. C., Greenberg R., Kolvoord R. A. 1994. Collisional lifetimes and impact statistics of near-Earth asteroids. In *Hazards due to comets and asteroids*, edited by Gehrels T. Tucson: University of Arizona Press. pp. 337–357.

Cathles L. M., Erendi A. H. J., and Barrie T. 1997. How long can a hydrothermal system be sustained by a single intrusive event? *Economic Geology* 92:766–771.

Collins G. S., Melosh H. J., Morgan J. V., and Warner M. R. 2002. Hydrocode simulations of Chicxulub crater collapse and peak-ring formation. *Icarus* 157:24–33.

Dmitriyev A. P., Kuzyayev L. S., Protasov Y. U. I., and Yamshchikov V. S. 1972. *Physical properties of rocks at high temperatures.* NASA Technical Translation, TT F-684.

Fletcher P. and Reimold W. U. 1989. Some notes and speculations on the pseudotachylites in the Witwatersrand basin and Vredefort dome, South Africa. *South African Journal of Geology* 92(3): 223–234.

Gibson R. L. 2002. Impact-induced melting of Archean granulites in the Vredefort dome, South Africa. I: Anatexis of metapelitic granulites. *Journal of Metamorphic Geology* 20:57–70.

Gibson R. L. and Jones M. Q. W. 2002. Late archaean to palaeoproterozoic geotherms in the Kaapvaal craton, South Africa: Constraints on the thermal evolution of the Witwatersrand basin. *Basin Research* 14:169–181.

Gibson R. L. and Wallmach T. 1995. Low pressure-high temperature metamorphism in the Vredefort dome, South Africa: Anticlockwise pressure-temperature path followed by rapid decompression. *Geological Journal* 30:319–331.

Gibson R. L. and Reimold W. U. 1999. The metamorphic fingerprint of large impact events: The example of the Vredefort dome, South Africa. *Meteoritics & Planetary Science* 34:A42–A43.

Gibson R. L., Reimold W. U., and Stevens G. 1998. Thermal-metamorphic signature of an impact event in the Vredefort dome, South Africa. *Geology* 26:787–790.

Goetze C. 1978. The mechanisms of creep in olivine. *Philosophical Transactions of the Royal Society of London Series A* 288:99–119.

Grieve R. A. F., Robertson P. B., and Dence M. R. 1981. Constraints on the formation of ring impact structures, based on terrestrial data. In *Multi-ring basins*, edited Merrill R. B. New York: Pergamon Press. pp. 37–57.

Grieve R. A. F. and Masaitis V. L. 1994. The economic potential of terrestrial impact craters. *International Geology Review* 36:105–151.

Grieve R. A. F. and Therriault A. 2000. Vredefort, Sudbury, Chicxulub: Three of a kind? *Annual Review of Earth and Planetary Science* 28:305–338.

Henkel H. and Reimold W. U. 1998. Integrated geophysical modelling of a giant, complex impact structure: Anatomy of the Vredefort structure, South Africa. *Tectonophysics* 287:1–20.

Jones M. Q. W. 1988. Heat flow in the Witwatersrand basin and environs and its significance for the South African shield geotherm and lithosphere thickness. *Journal of Geophysical Research* 93:3234–3260.

Kamo S. L., Reimold W. U., Krogh T. E., and Colliston W. P. 1996. A 2.023 Ga age for the Vredefort impact event and a first report of shock metamorphosed zircons in pseudotachylitic breccias and granophyre. *Earth and Planetary Science Letters* 144:369–387.

Keith T. E. C., White D. E., and Beeson M. H. 1978. Hydrothermal alteration and self-sealing in Y-7 and Y-8 drill holes in northern part of Upper Geyser basin, Yellowstone National Park, Wyoming. *Geological Survey Professional Papers* 1054-A:26.

Keszthelyi L. and Denlinger R. 1996. The initial cooling of pahoehoe flow lobes. *Bulletin of Volcanology* 58:5–18.

Kirby S. H. and Kronenberg A. K. 1987. Correction to "Rheology of the lithosphere: Selected topics." *Reviews of Geophysics* 25: 1680–1681.

Koeberl C., Reimold W. U., and Shirley S. B. 1996. Re-Os isotope and geochemical study of the Vredefort granophyre: Clues to the origin of the Vredefort structure, South Africa. *Geology* 24(10): 913–916.

Leroux H., Reimold W. U., and Doukhan J. 1994. A TEM investigation of shock metamorphism in quartz from the Vredefort dome, South Africa. *Tectonophysics* 230:223–239.

Maxwell D. and Seifert K. 1975. Modeling of cratering, close-in displacements, and ejecta. Washington, D.C.: Defense Nuclear Agency

McCarthy T. S., Stanistreet I. G., and Robb L. J. 1990. Geological studies related to the origin of the Witwatersrand basin and its mineralization—An introduction and a strategy for research and exploration. *South African Journal of Geology* 93(1):1–4.

Melosh H. J. 1977. Crater modification by gravity: A mechanical analysis of slumping. In *Impact and explosion cratering*, edited by Roddy D. J., Pepin R. O., and Merrill R. B. New York: Pergamon Press. pp. 1245–1260.

Melosh H. J. 1982. A schematic model of crater modification by gravity. *Journal of Geophysical Research* 87:371–380.

Melosh H. J. and Raefsky A. 1980. The dynamical origin of subduction zone topography. *Geophysical Journal of the Royal Astronomical Society* 60:333–354.

Newsom H. E. 1980. Hydrothermal alteration of impact melt sheets with implications for Mars. *Icarus* 44:207–216.

Newsom H. E., Britelle G. E., Hibbits G. A., Crossey L. J., and Kudo A. M. 1996. Impact crater lakes on Mars. *Journal of Geophysical Research* 101(E6):14951–14956.

Nicolaysen L. O., Hart R. J., and Gale N. H. 1981. The Vredefort radioelement profile extended to supracrustal strata at Carletonville, with implications for continental heat flow. *Journal of Geophysical Research* 86:10653–10661.

O'Brien D. P., Geissler P., and Greenberg R. 2001. A melt-through model for chaos formation on Europa. *Icarus* 156:152–161.

Osinski G. R., Spray J. G., and Lee P. 2001. Impact-induced hydrothermal activity within the Haughton impact structure, arctic Canada: Generation of a transient, warm, wet oasis. *Meteoritics & Planetary Science* 36:731–745.

Pierazzo E. and Melosh H. J. 2000. Melt production in oblique

impacts. *Icarus* 145:252–261.
Pierazzo E., Vickery A. M., and Melosh H. J. 1997. A re-evaluation of impact melt production. *Icarus* 127:408–423.
Reimold W. U. and Wallmach T. 1991. The Vredefort structure under discussion. *South African Journal of Science* 87:412–417.
Rondot J. 1994. Recognition of eroded astroblemes. *Earth Science Reviews* 35:331–365
Schmid S. M., Boland J. N., and Paterson M. S. 1977. Superplastic flow in fine-grained limestone. *Tectonophysics* 43:257–291.
Schmidt R. M. and Housen K. R. 1987. Some recent advances in the scaling of impact and explosion cratering. *International Journal of Impact Engineering* 5:543–560.
Stevens G., Gibson R. L., and Droop G. T. R. 1997. Mid-crustal granulite facies metamorphism in the Central Kaapvaal craton: The Bushveld complex connection. *Precambrian Research* 82: 113–132.
Therriault A. M., Grieve R. A. F., and Reimold W. U. 1997. Original size of the Vredefort structure: Implications for the geological evolution of the Witwatersrand basin. *Meteoritics & Planetary Science* 32:71–77.
Thompson S. L. 1979. CSQIII An Eulerian finite differences program for two-dimensional material response: User's manual. Sandia National Laboratories, New Mexico.
Thompson S. L. and Lauson H. S. 1972. Improvements in the chart D radiation-hydrodynamic code III: Revised analytical equation of state. Sandia National Laboratories, New Mexico.
Turtle E. P. and Pierazzo E. 1998. Constraints on the size of the Vredefort impact crater from numerical modeling. *Meteoritics & Planetary Science* 33:483–490.
Turcotte D. L. and Schubert G. 1982. *Geodynamics: Applications of continuum physics to geological problems*. New York: Wiley and Sons.